Tight-binding model of selenium disordered phases

D. Molina and E. Lomba

Instituto de Química Física Rocasolano, CSIC, Serrano 119, E-28006 Madrid, Spain

G. Kahl

Institut für Theoretische Physik and CMS, Technische Universität, Wiedner Hauptstrasse 8-10, A-1040 Wien, Austria

Following the parametrization scheme first introduced by Goodwin, Skinner, and Pettifor, we propose here a model of the empirical tight-binding Hamiltonian for selenium, based on the fitting of cohesive energy curves obtained from density-functional calculations for solid phases, rings, and chains structures. We have assessed the model by means of various tight-binding molecular-dynamics calculations performed in liquid and amorphous states. Comparisons with *ab initio* calculations and experimental results indicate that the model is fairly accurate for the pair structure at low and medium temperatures, but tend to overestimate bonding at high temperatures. The number of valence alternation pair defects also seems to be overestimated. On the other hand, the band structure derived from the tight-binding density of states predicts the occurrence of a semiconductor-to-metal transition when approaching the critical temperature in good agreement with *ab initio* calculations and experimental evidence. [S0163-1829(99)02333-4]

I. INTRODUCTION

A great deal of work has been dedicated in recent years to elucidate the electronic structure of liquid and amorphous selenium and its interplay with the structural changes occurring upon melting and when approaching the critical point. Together with various neutron[1,2] and x-ray-diffraction experiments,[3,4] a large amount of theoretical work has been invested from different levels of approximation ranging from pure *ab initio* calculations,[5–10] to simple tight binding (TB) models,[11–13] as well as effective potential calculations.[14,15] Useful techniques like the reverse Monte Carlo (RMC) method[16] have come to aid the elucidation of the structure obtained from diffraction experiments.[17] However, despite the wealth of data and numerous discussions, a number of issues remain somewhat unsettled for the following reasons. First, diffraction experiments offer mostly information on the pair structure, and although the RMC furnishes a deep insight into the atomic structure compatible with experimental structure factors, some fine details in the structure [like the number of valence alternation pairs (VAP's), responsible for the small response of the electronic behavior of Se to doping] are too subtle to get an unequivocal answer. On the other hand, pure *ab initio* calculations have been mostly done in the local-density approximation (LDA),[18] although recently some generalized gradient corrections (GGA) have also been incorporated. The limitations of the LDA are well known (excess of correlation, incorrect gap sizes) and it is also known that GGA tends to overcorrect the defficiencies of the LDA.[19] In any case, recent calculations have shown that this type of approach is well suited to treat liquid Se,[8–10] despite the fact that its most important limitation is the restriction to small sample sizes, due to the high computational cost of the calculation. Therefore we have considered worth revisiting the empirical tight-binding approximation, following the ideas that Goodwin, Skinner, and Pettifor (GSP) successfully exploited in the case of silicon.[20] Since Se is a covalent semiconductor with strongly localized bonds, the TB approach seems promising, as previous works by Bichara, Pelegatti, and Gaspard[11] have shown using a relatively simplistic parametrization. A basic parametrization for the TB Hamiltonian of Se was proposed years ago by Robertson[13] by simultaneously fitting *s*- and *p*-band shapes obtained in the LDA for trigonal Se and the experimental optical gap. Following GSP, this parametrization has to be complemented with a series of terms that guarantee the transferability of the Hamiltonian to various structures, plus a set of parameters that should model the repulsive interactions, where core-core and electron-electron interactions are included in an effective way. The fitting parameters should then render cohesive energy curves in agreement with *ab initio* calculations for the largest possible set of clusters, chains, and crystalline phases. This is the approach we have followed here. Once the model Hamiltonian was defined, our purpose was to put it to a stringent test in the liquid and amorphous phases. To this aim, we have carried several molecular-dynamics (MD) simulations where the dispersive forces have been evaluated via the Hellmann-Feynman theorem by means of the full diagonalization of the Hamiltonian. A representative sample of 162 atoms has been used in most cases. This is obviously too small to give a correct account of the chain dynamics, but it has proven sufficient to check the model Hamiltonian which is the central aim of this work. As will be shown in the following pages, we can say that the model has passed the test. The agreement with experimental results for the structure factors is fair over a wide range of temperatures. The same can be said when comparing with *ab initio* results, except for the tendency in the TB model to encourage bonding at high temperatures. Diffusion constants seem to be in relatively good accordance with *ab initio* calculations, and most crucially, this TB model predicts a semiconductor-to-metal transition when approaching the critical point due to band crossing. This whole picture agrees remarkably well with experimental results, which illustrates the usefulness of TB Hamiltonian and the TB-MD technique to describe liquid and amorphous covalent semiconductors.

PRB <u>60</u>   6372

The rest of the paper is sketched as follows. In the next section we summarize the essential features of the TB modeling and present our TB Hamiltonian derived from the fitting to various structures. In Sec. III we give a brief summary of the simulation details. Then, Secs. IV, V, and VI present the core of our results for the atomic structure, diffusion constants, and band structure. Finally, some conclusions and future prospects are presented in Sec. VII.

II. TIGHT-BINDING MODEL

The functional forms of the hopping integrals in the standard empirical TB Hamiltonians are well known since the work of Harrison.[21] Nonetheless, to guarantee transferability, in this work we have subscribed to the approach proposed by Goodwin, Skinner, and Pettifor[20] to model silicon. These authors formulate functionals for hopping integrals consistent with Harrison's $1/r^2$ decay and repulsive pair interactions to enforce mechanical stability. The priority was set on extending the transferability of the Hamiltonian to account for properties of close-packed structures within the framework of the tight-binding approximation. In the case of silicon, a rather small number of parameters was enough to reproduce its properties over a wide range of physical conditions, representing the most probable local coordinations. On the other hand, when this approach was applied to carbon by Xu et al.,[22] it was necessary to increase the number of parameters by a factor of 2, incorporating nonpairwise additive repulsive forces to correctly account for a few common structures. This is due to the fact that in the case of carbon one has to take into account structures from linear chains to close-packed phases, and the former are somewhat hard to model with purely pair repulsive interactions.

The case of selenium is also somewhat delicate since it occurs as twofold coordinated for most of the accesible physical conditions. Transferability here has to focus mostly on the hopping to second neighbors since the first-neighbor shell is essentially constant on most phases. Anyway, it is important to take into account close-packed structures in order to guarantee at least that these phases do not interfere with the most stable ones: rings, chains, and trigonal structures.

Following the TB approach in the treatment of Goodwin, Skinner, and Pettifor,[20] we split the potential energy of the system in a contribution stemming from the valence electrons E_b and a repulsive term derived from the screened Coulombic repulsion and the exclusion principle between core states E_{rep}. This term is assumed to be pairwise additive. Thus one has

$$E = E_b + E_{rep},$$

$$E_b = 2 \sum_i^{n_{occ}} \epsilon_i,$$ (1)

$$E_{rep} = \sum_{i<j} u^{rep}(R_{ij}),$$

where ϵ_i are the one-electron eigenvalues of the TB Hamiltonian, n_{occ} is the occupation number, and

$$u^{rep}(r) = \varphi_0 (d_0/r)^m \exp\{m[-(r/d_c)^{m_c} + (d_0/d_c)^{m_c}]\}.$$ (2)

In the independent electron approximation the valence electron Hamiltonian H can be decomposed in $n = zN$ (N is the number of atoms and z the valence number) terms

$$H = \sum_i^n h_i,$$ (3)

where the one-electron Hamiltonian h (for simplicity we omit the subscript i) is

$$h = \sum_{p,\alpha} \epsilon_p^\alpha a_{p,\alpha}^+ a_{p,\alpha} + \sum_{p \neq q, \alpha, \beta} t^{\alpha\beta}(|\mathbf{R_p} - \mathbf{R_q}|) a_{p,\alpha}^+ a_{q,\beta}.$$ (4)

Here, $\epsilon_p^\alpha = \epsilon^\alpha$ are the on-site energies of the valence electrons in the basis set chosen, $t^{\alpha\beta}(|\mathbf{R_p} - \mathbf{R_q}|)$ are the energies associated to electron hopping from state α in the atom located in $\mathbf{R_p}$ to state β in the atom in $\mathbf{R_q}$. $a_{p,\alpha}^+$ ($a_{q,\alpha}$) are the corresponding creation (anihilation) operators defined in terms of atom-centered basis functions. Following GSP, the radial factor of hopping integrals can be parametrized as

$$t^{\alpha\beta}(r) = t_0^{\alpha\beta}(r_0/r)^n \exp\{n[-(r/r_c^{\alpha\beta})^{n_c^{\alpha\beta}} + (r_0/r_c^{\alpha\beta})^{n_c^{\alpha\beta}}]\}.$$ (5)

The values of $t_0^{\alpha\beta}$ and r_0 have been taken from the original parametrization of Robertson[13] while other parameters in Eqs. (2) and (5) will be treated in the GSP spirit. However, in contrast with the original GSP treatment each hopping term will be modeled separately, incorporating different decays (i.e., $r_c^{\alpha\beta}$ and $n_c^{\alpha\beta}$) for each term. This peculiarity has its origin in the fact that in contrast with the parametrization for group IV elements, Robertson's treatment of group V and VI includes hopping terms to second neighbors. To be consistent with this, $r_c^{\alpha\beta}$ and $n_c^{\alpha\beta}$ have to be adjusted independently for each hopping interaction. On the other hand, the GSP hopping functions do not decay rapidly enough to guarantee that only up to third neighbors are taken into account. Therefore following Xu et al.,[22] we introduce extra parameters $r_2^{\alpha\beta}$ (larger than the second-neighbor distance), such that the functional forms $t^{\alpha\beta}(r)$ are replaced for $r_2^{\alpha\beta} < r < R_c^{\alpha\beta}$ (the absolute cutoff) by polynomial functions

$$s^{\alpha\beta}(r) = \sum_{n=0}^3 c_n^{\alpha\beta} r^n,$$ (6)

where the coefficients $c_n^{\alpha\beta}$ are calculated by imposing the following conditions:

$$t^{\alpha\beta}(r_2^{\alpha\beta}) = s^{\alpha\beta}(r_2^{\alpha\beta}), \quad \left.\frac{\partial t^{\alpha\beta}(r)}{\partial r}\right|_{r_2^{\alpha\beta}} = \left.\frac{\partial s^{\alpha\beta}(r)}{\partial r}\right|_{r_2^{\alpha\beta}},$$

$$s^{\alpha\beta}(R_c^{\alpha\beta}) = 0, \quad \left.\frac{\partial s^{\alpha\beta}(r)}{\partial r}\right|_{R_c^{\alpha\beta}} = 0,$$ (7)

that guarantee a smooth decay of the interactions at a given cutoff, which is essential in a MD simulation, as well as an adequate connection of the polynomial to the corresponding hopping function.
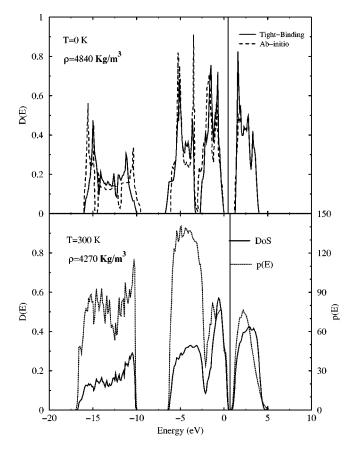
FIG. 1. Electronic density of states of the trigonal phase. With solid line, the tight-binding curve, calculated by integration over the reciprocal space using randomly chosen 10 000 k vectors of the reciprocal unit cell. With dashed line, DOS calculated by LDA +GGA taken from Ref. 7 (top). In the supercooled state (bottom) the DOS is plotted together with the participation ratio, $p(E)$ (dotted line and ordinates on the right).

This procedure was carried out paying special attention to the *ab initio* electronic density of states (DOS) in the trigonal phase,[7] in particular to the shape of the bonding-σ and nonbonding-π valence bands. In order to keep a good agreement with the *ab initio* DOS, the second-neighbor hoppings ($t_1^{\alpha\beta}$) have been modified with respect to Robertson's original values. Note that once the value of the hopping is also set at the second-neighbor distance (r_1), the parameters of the GSP functional form have to verify the following equations:

$$t^{\alpha\beta}(r_0)=t_0^{\alpha\beta}, \quad t^{\alpha\beta}(r_1)=t_1^{\alpha\beta}, \quad (8)$$

reducing in this way the number of free parameters during the cohesive energy fitting.

Finally, we have to mention that in the Robertson's parametrization,[13] there is a splitting in the site energies of p orbitals depending on the σ or π nature of the bonding. This splitting cannot be incorporated on a TB treatment based on Hamiltonian diagonalization. Thus, whereas we manage to reproduce satisfactorily the *ab initio* DOS (see Fig. 1), results for the size of the gap in the trigonal phase are somewhat worse than those of Robertson.

Then, as mentioned above, we take from Robertson[13] the values of hopping at 2.37 Å (first-neighbor distance) and obtain the remaining parameters by fitting to cohesive energy
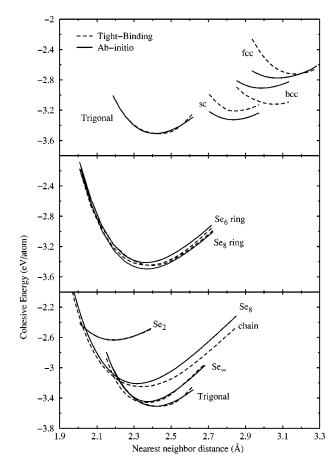

FIG. 2. Tight-binding fitting of twofold coordinated phases (bottom and center) and cubic phases (above). Cohesive energy per atom vs nearest-neighbor distance. Curves calculated by LDA +GGA are denoted with solid lines and with dashed lines, the TB fit.

curves calculated by means of density-functional theory, with the second-neighbor hopping values ($t_1^{\alpha\beta}$ at 3.44 Å) adjusted to fit the *ab initio* DOS in the trigonal phase.[8,23] The repulsive pair potential parameters are also calculated during the fitting, with fewer restrictions than their hopping counterparts.

The *ab initio* cohesive energy curves were calculated by the Vienna *ab initio* Simulation Package (VASP) (Ref. 24) and all corrections needed to give a good account of the peculiarities of selenium were included. More details can be found in Ref. 7. As seen in Fig. 2, we have represented cohesive energies vs nearest-neighbor distance. However, the volume expansion of the different structures is carried out in various ways depending on the structure considered, in order to avoid the imposition of artificial structural trends in the model. Therefore in addition to the nearest-neighbor distance, some structures need extra parameters to be completely defined. The volume variation of six- and eight-atom rings, the eight-atom chain, and the trigonal phase consists just in a uniform expansion of the minimum energy configurations. On the other hand, the infinite chain is created by distortion of the hexagonal cell in the trigonal phase, where the separation between chains has been doubled. The volume expansion here affects only the z axis of the trigonal cell (parallel to the chain) and consequently bond angles are dis-

TABLE I. Set of TB parameters for selenium used in the model proposed in this work.

t_0^{ss} (eV)	t_1^{ss} (eV)	n^{ss}	n_c^{ss}	r_c^{ss} (Å)	r_0^{ss} (Å)
−1.11	-0.20	2.0	1.000	2.2093	2.37
r_2^{ss} (Å)	c_0^{ss}	c_1^{ss}	c_2^{ss}	c_3^{ss}	R_c^{ss} (Å)
3.4437	0.179197	−0.266293	−2.739557	5.824826	3.8
t_0^{sp} (eV)	t_1^{sp} (eV)	n^{sp}	n_c^{sp}	r_c^{sp} (Å)	r_0^{sp} (Å)
2.10	0.05	2.0	1.700	1.7391	2.37
r_2^{sp} (Å)	c_0^{sp}	c_1^{sp}	c_2^{sp}	c_3^{sp}	R_c^{sp} (Å)
3.5536	0.015531	−0.058817	−0.290135	1.108101	3.8
$t_0^{pp\sigma}$ (eV)	$t_1^{pp\sigma}$ (eV)	$n^{pp\sigma}$	$n_c^{pp\sigma}$	$r_c^{pp\sigma}$ (Å)	$r_0^{pp\sigma}$ (Å)
3.37	0.61	2.0	1.160	2.6168	2.37
$r_2^{pp\sigma}$ (Å)	$c_0^{pp\sigma}$	$c_1^{pp\sigma}$	$c_2^{pp\sigma}$	$c_3^{pp\sigma}$	$R_c^{pp\sigma}$ (Å)
3.5850	0.145638	−0.217066	−1.491211	2.815979	4.0
$t_0^{pp\pi}$ (eV)	$t_1^{pp\pi}$ (eV)	$n^{pp\pi}$	$n_c^{pp\pi}$	$r_c^{pp\pi}$ (Å)	$r_0^{pp\pi}$ (Å)
-0.92	-0.35	2.0	10.00	4.2767	2.37
$r_2^{pp\pi}$ (Å)	$c_0^{pp\pi}$	$c_1^{pp\pi}$	$c_2^{pp\pi}$	$c_3^{pp\pi}$	$R_c^{pp\pi}$ (Å)
3.4405	0.380214	−0.471939	−1.956430	2.833510	4.0
φ_0 (eV)	m	m_c	d_c (Å)	d_0 (Å)	R_c^{rep} (Å)
3.2830	4.6085	1.6358	3.5993	2.44	3.8
d_2 (Å)	c_0^{rep}	c_1^{rep}	c_2^{rep}	c_3^{rep}	
3.4000	0.122608	−0.413844	−0.229670	1.244951	
ϵ_s (eV)	ϵ_p (eV)				
−12.41	−1.50				

torted, contrary to the expansion of the eight-atom chain. Curves for other solid phases (sc, bcc, and fcc), as well as the dimer (see Fig. 2), have also been calculated and although they correspond to energetically unfavored structures, they still have to be taken into account to a certain extent during the fitting, as will be seen in more detail below.

The fitting procedure was performed by a random minimization method (simplex) of the mean-square deviation between *ab initio* and tight-binding energies. Energies of the solid phases have been calculated from the repulsive energies plus the band energies evaluated using special **k** points suited to each solid structure.[25] In a multiparameter fitting like this, it is extremely easy to hit local minima and unphysical results, therefore we have been particularly careful to impose certain constraints so as to guide the minimization procedure. The most obvious conditions should force the precise location of the minima and preserve the relative energetic ordering of the most likely structures, in order to avoid undesirable transitions. All this constraining was achieved by imposing various weighting factors to each structure and overweighting the regions around the energy minima. The parameters finally obtained are summarized in Table I and the cohesive energy curves compared with *ab initio* calculations can be seen in Fig. 2.

III. SIMULATION DETAILS

In order to thoroughly check the model proposed here, we have performed simulations in the liquid and amorphous phases for the set of thermodynamic states listed in Table II. For most of these conditions both experimental and *ab initio* results are available in the literature. As previously mentioned, the simulation technique is tight-binding molecular-dynamics (TB-MD). Following Wang, Chan, and Ho[26] and Virkunnen, Laasonen, and Nieminen,[27] for each configuration the TB Hamiltonian is diagonalized and the forces on each particle are evaluated via the Hellmann-Feynman theorem to yield

TABLE II. Conditions of TB-MD simulation runs in this work.

T(K)	ρ(g/cm^3)	n(Å^{-3})	t_{equ}(ps)	t (ps)
300	4.27	0.0326	13.91	10
570	3.9	0.0297	5.54	10
870	3.69	0.0281	5.21	8
1370	3.29	0.0251	5.50	7
1770	3.11	0.0237	5.71	9

TABLE III. CPU times per step (Processor Intel Pentium II at 450 MHz.). Notice that the dimension of the matrix to be diagonalized is four times the number of particles, since we are working with an sp^3 basis.

No. atoms	CPU time/step (s)
48	0.343
162	16.070
400	265.248

$$\mathbf{F_i} = \sum_{j \neq i} \frac{\partial u^{rep}(R_{ij})}{\partial \mathbf{R_{ij}}} + \sum_{n}^{n_{occ}} \sum_{j \neq i, \alpha, \beta} c_i^{\alpha (n)} c_j^{\beta (n)} \left(\frac{\partial t^{\alpha\beta}(R_{ij})}{\partial \mathbf{R_{ij}}} \right) \tag{9}$$

with

$$\Psi^{(n)}(\mathbf{r}) = \sum_{\alpha, i} c_i^{\alpha} \phi^{\alpha}(\mathbf{r} - \mathbf{R_i}) \tag{10}$$

being the one-electron eigenfunction. Equations of motion are then solved using a standard predictor-corrector algorithm with a time step of 1 fs. As seen in Eq. (9) when evaluating the forces, sampling on $\mathbf{k}$ space for the disordered system reduces to the Γ point. The simulations were done on systems of 162 atoms in the microcanonical ensemble starting from a cubic simulation cell. The diagonalization has been carried out using a standard divide and conquer algorithm[28] which has proven to be extremely efficient for this type of problem. Information about CPU times (in an Intel Pentium II processor at 450 MHz) is shown in Table III. A standard run then reduces to 70 h of CPU time in an inexpensive desktop computer, well below the demands of the simplest DFT calculations. One finds that CPU timing scales as N^3, which obviously depend directly on the diagonalization strategy to be followed. As in the case of *ab initio* calculations, order-N methods will provide an alternative to cope with large systems.[30] Samples were equilibrated for 5 ps and then evolved freely during 10 ps. For the supercooled regime the sample had to be prepared more carefully, first equilibrating the system at 600 K during 3 ps and, second, cooling down and equilibrating to 300 K for 10 ps. The production run was then continued for 10 ps more. Nonetheless, the state obtained is not really amorphous, given its small but nonzero diffusion constant and one should more properly speak of a subcooled liquid. The energy drift of the simulations is around 0.003% over the whole run and fluctuations in temperature were below 5%.

IV. STRUCTURE

As a first test of our model we have analyzed its structural predictions, focusing both on the pair structure, angular correlations, and clustering. It will be shown here that the proposed model is particularly suitable to describe the regions of phase space corresponding to low and medium temperatures, exhibiting the most apparent discrepancies at high temperatures due to a tendency to overestimate bonding.
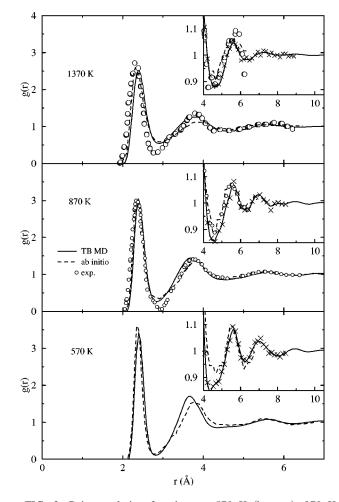

FIG. 3. Pair-correlation functions at 570 K (bottom), 870 K (middle), and 1370 K (top). Results from inversion of neutron-scattering data from Ref. 1 are denoted by hollow circles, *ab initio* calculations from Ref. 8 by dashed curves, and TB-MD simulations are denoted by solid curves. The inset illustrates the long-range behavior of the PCF, where the crosses correspond to the bare TB-MD results and the solid line is the result of their extension via Verlet's procedure.

A. Pair structure

In this section, we compare our results in the liquid and supercooled states with *ab initio* and experimental data when available. In Fig. 3, the pair-correlation functions (PCF) of liquid selenium are compared with *ab initio*[8] (at 570, 870, and 1370 K) and experimental results[1] when available. The structure factors are shown in Fig. 4 (at 300 and 570 K) and in Fig. 5 (at 870, 1370, and 1770 K), compared with neutron scattering,[1,2] x-ray diffraction,[3] and *ab initio* data.[8] In the latter case, structure factors have been obtained by extension of the simulated pair distribution functions using the procedure described below.

First, if we focus on the PCF's, it can be easily appreciated that the accordance with *ab initio* and experimental results is rather good. The TB-MD data for the first-neighbor shell agrees remarkably well with *ab initio* calculations at all conditions, what can be understood as a consequence of the accuracy of the TB fitting in the neighborhood of the potential minima. The only deficiency of our model in this region can be observed in a small shift in the position of the
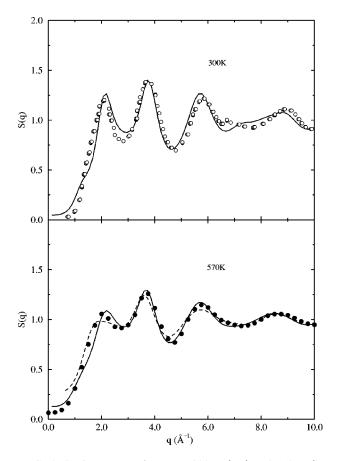
FIG. 4. Static structure factors at 300 K (top) and 570 K (bottom). Neutron-scattering experiments data from Ref. 2 are plotted with hollow circles. The x-ray diffraction data are taken from Ref. 3 (black circles). The *ab initio* structure factors are from Ref. 8 and are represented by dashed lines. Finally, TB-MD simulation results are denoted by solid lines.

maxima resulting from a corresponding shift in the minima of the energy curves that can be seen in Fig. 2.

When we concentrate on the second-neighbor shell, the TB nature of our model becomes particularly patent. The excess of bonding in the TB model enforces higher localization and the second-shell becomes more structured and constrained to a smaller range. When integrated up to its second minimum, the PCF yields a coordination number for the second neighbor distance somewhat larger than the experimental estimates. This is particularly patent for the supercooled system for which we obtain 7.8 neighbors vs 6.8, the experimental value in an amorphous state.[33] Unfortunately, we ignore the way in which the experimental value has been calculated and so comparisons are only qualitative. In any case, we will see that this is the result of an excess of threefold coordination which is not reflected in the first-neighbor shell due to averaging with onefold coordination (i.e., formation of VAP's). However, when compared to experimental PCF's, the peak positions are reproduced more accurately than by *ab initio* calculations, which is somewhat fortuitous.

Finally, in the long range we can still see oscillations which extend over several coordination shells at all temperatures. That is a certain sign of the existence of highly correlated quasimolecular structures, with atoms strongly bonded. Particularly at high temperatures, this tendency seems to be overestimated by our model, which supports a picture of ex-
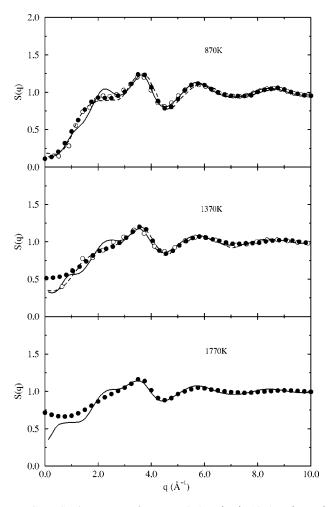

FIG. 5. Static structure factors at 870 K (top), 1370 K (center), and 1770 K (bottom) from neutron-scattering experiments from Ref. 1 (hollow circles), from x-ray diffraction experiments from Ref. 3 (black circles), and from TB-MD simulations (solid lines). *Ab initio* results from Ref. 8 are denoted by dashed lines.

cessively long chains. We believe that the inclusion of a Hubbard-like term will favor the chain shortening and reduce the threefold coordination improving the structural predictions. This will be the subject of future work. At this point, we have to stress the importance of these long-range correlations to get accurately the decay of structure factors at low-**k** vector. In our simulations the sample size was large enough to guarantee the reliability of the results. In any case, we have extended the simulated PCF by means of Verlet's procedure,[31] which implies the solution of the Orstein-Zernike equation

$$h(r_{12}) = c(r_{12}) + \rho \int c(r_{13}) h(r_{32}) d\mathbf{r_3} \qquad (11)$$

with $h(r) = g(r) - 1$ and the direct correlation function given by

$$c(r) = g^{MD}(r) - 1 - [h(r) - c(r)], \quad r \leqslant R_c,$$

$$c(r) = f(r), \quad r > R_c, \qquad (12)$$

where $R_c = L/2$ with L being the side of simulation box and $g^{MD}(r)$ the PCF extracted from the simulation results. $f(r)$

can be set to zero, or to some r-decaying function. Here we have just used $f(r) = c(R_c)R_c^6/r^6$, which provided a smooth transition at the discontinuity, affecting only the $k=0$ behavior of the structure factor, which has been removed from the figures.

All the features observed in the PCF's have their counterpart in the structure factor. The main deviations appear in the low-**k** region at medium and high temperatures, where correlations with a large spatial periodicity are clearly overestimated. That means that our model will be unable to mimic the critical behavior and that is also why we emphasize the importance of including a charge-charge repulsion term to reduce these correlations. The rest of the structure factor is in very good agreement with experimental results at all temperatures, except for little shifts in its phase, which result from the somewhat incorrect estimation of the bond length by both TB and *ab initio* calculations in liquid and supercooled states.

B. Clustering and coordination analysis

With the aim of going beyond the pair structure, we have performed clustering and coordination analysis on the simulation configurations. Results here are merely qualitative, since we have disregarded the distortion introduced by thermal vibrations on the structure.[32] We have defined the bond length at every temperature in terms of the location of the first minimum in the respective PCF. Paying attention to the coordination number, one can split it in four contributions, corresponding to isolated ($0F$), onefold ($1F$), twofold ($2F$), and threefold ($3F$) coordinated sites. In order to give a more precise idea of what is going on at each temperature, we have performed two different types of analysis of the history of every simulation. In Fig. 6 (top), we can observe the normalized distribution of the average coordination number $N(\langle N_C \rangle)/N$. This quantity is obtained calculating the average coordination number ($\langle N_C \rangle$) of each and every particle in the sample along the simulation and then sorting the particles according to the value of $\langle N_C \rangle$, thus getting $N(\langle N_C \rangle)/N$. On the other hand, in Fig. 6 (bottom), we have plotted the average coordination distribution ($\langle N(N_C) \rangle/N$) that accounts for the distribution of atoms N_C fold coordinated at every time step, on the average. As can be seen, the differences between both charts increase with temperature. Somehow, this provides an intuitive estimation of the bond lifetime. At low temperatures, similarities between both diagrams indicate the existence of well defined defects with a long lifetime. On the other hand, at high temperatures, discrepancies imply a picture of bonds breaking and being created rapidly so that each atom, on the average, appears to be twofold coordinated, whereas the average of the instantaneous distribution indicates that the sample will be formed by short-lived three-dimensional entanglements of atoms. Another important point is the considerable number of defects ($1F$ and $3F$ atoms) at all temperatures, seemingly more stable at low and medium temperatures, where most of the $3F$ and $1F$ sites occur in VAP's. These data are in contrast to *ab initio* results, where the number of $2F$ atoms is around 90% at 570 K.[9]

The cause of this disagreement might be traced back to the TB nature of our model. As we explained before, the TB
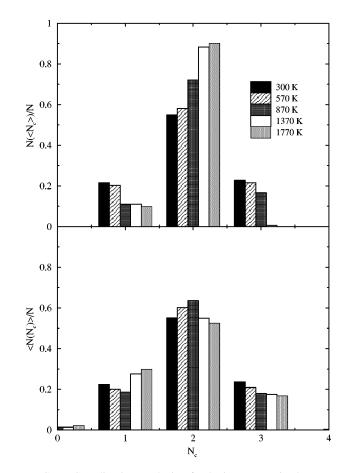

FIG. 6. Coordination analysis of selenium atoms in the supercooled phase at 300 K and in the liquid phases at 570, 870, 1370, and 1770 K. Distribution of atoms with a given average coordination number is plotted at top. At bottom, the bar chart represents the average distribution of atoms n-fold-coordinated.

model disregards electron-electron correlations (as a result of the independent electron approximation) and consequently induces an excess of charge transfer. All threefold coordinated atoms are positively charged and onefold coordinated atoms have an excess of electrons in lone pairs. Since electron-electron repulsions are neglected, the weight of these configurations might be overestimated in comparison with neutral twofold coordinated chains. These latter structures are absolutely dominant in the *ab initio* results, in which electron-electron correlation are in fact included. In a forthcoming work, the influence of a Hubbard-like term to minimize charge transfers will be studied.

Nonetheless, since very divergent microscopic descriptions are able to give the same pair structure, it would be desirable to get some further experimental information on the nature of bonding and the microscopic structure at low T. In this regard, reverse Monte Carlo calculations carried out by Petkov and Yunchov,[17] seem to produce a microscopic picture in better agreement with the percolating three-dimensional network predicted by our TB model.

C. Bond angle structure

Bond angle distributions (BAD) in the liquid state are shown in Fig. 7. The criterion to define the bond length is exactly the same as used before. The values obtained here
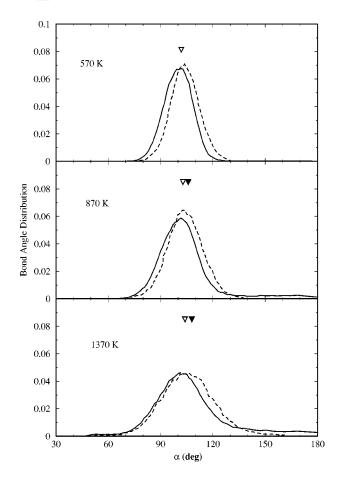
FIG. 7. Bond angle distributions at 570, 870, and 1370 K. TB-MD results are denoted by solid line. *Ab initio* BAD's for twofold-coordinated atoms are plotted in dashed lines. The average bond angles extracted from x ray (Ref. 4) and neutron scattering (Ref. 1) are shown as hollow and black triangles, respectively.

are in good agreement with diffraction experiments. However, it should be born in mind that experimental values have been estimated under the very rough assumption that the first and second peaks in the PCF are associated with the average first and second intrachain neighbor distances, respectively. This introduces some uncertainty as regards the accuracy of the experimental estimates. Additionally, *ab initio* BAD's (Ref. 8) have been calculated separately for $2F$ and $3F$ atoms, in contrast with our distribution, averaged over the whole sample, which might account to a certain extent for the observed deviations. In any case these departures are well within the uncertainties of the simulation.

V. DYNAMICAL PROPERTIES

Dynamics is perhaps one of the most interesting physical aspects of liquid and amorphous Se, being markedly determined by the existence of long chains. It is here where a good TB model can have a larger impact, due to the advantages in computation time and storage of this kind of simulation with respect to pure *ab initio* calculations. At this stage, we will only concentrate on one of its simplest aspects, i.e., the diffusion phenomena, in order to compare with available *ab initio* data. A full study of the dynamics of this TB model of selenium (from phonon dispersion curves

TABLE IV. Self-diffusion constants (units of 10^{-9} m^2/s) in the TB-MD of selenium compared with *ab initio* results from Ref. 8 and experimental results from Refs. 34 and 35.

T(K)	This work	*Ab initio*	Exp. (Ref. 34)	Exp. (Ref. 35)
300	0.20			
570	1.21	0.5	0.4	0.2
870	4.11	3.5	1.9	22.0
1370	16.02	17.5	5.4	

to viscosity) will also be the subject of a future work. In this section we will just discuss the diffusion and the influence of the finite size on that calculation. Self-diffusion constant is evaluated here through the Einstein equation which governs the time evolution of the mean-square displacement (MSD) per particle in the infinite time limit, which follows:

$$\langle r^2(t)\rangle - \langle r^2(t=0)\rangle = 6\eta t + \text{const}, \qquad (13)$$

where η is the diffusion constant and t is the time. The calculated values for all states considered are reported in Table IV and in Fig. 8 we have plotted the evolution in time of the MSD. Here the TB-MD seems to agree reasonably well with the *ab initio* calculations. However, the results at 570 K suffer from a certain lack of statistics since, in ten picoseconds, atoms hardly move the equivalent to a nearest-neighbor distance, and the same can be said about the *ab initio* results. The fact that at 1370 K one gets a TB diffusion constant smaller than the *ab initio* value in contrast with the low-temperature situation, is probably due to the persistence of long chains in the TB high-temperature sample, which tend to break in smaller units in the *ab initio* calculation. We note in passing that the value obtained here at 570 K (1.21×10^{-9} cm^2/s) is in better accordance with the *ab initio* value obtained via the velocity autocorrelation function.[8] To evaluate the importance of the sample size in the self-diffusion constant calculation, we performed a simulation with 48 atoms at 1370 K. Despite the remarkable decrease in sample size (and hence in absolute chain length), diffusion
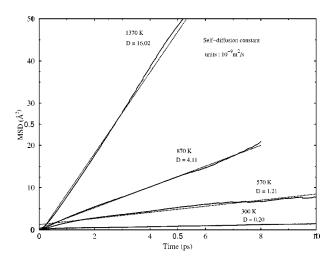

FIG. 8. Mean-square displacement curves from TB-MD simulations at 300, 570, 870, and 1370 K. Diffusion constants calculated by a least-squares fitting (with dashed lines) are also collected and compared with *ab initio* results in Table IV.
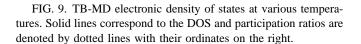
constants only diminish 10%. As to the 300-K state, some diffusion is still observed and consequently it should be considered as a supercooled liquid, though as a first approximation might well be compared with experimental results for a really amorphous state. The analysis of diffusion constants stresses again how rather different microscopic pictures are able to reproduce in good agreement several physical properties, especially those that could be more sensitive to the microscopic differences between both descriptions, which somehow indicates that the leading influence of the pair structure and thermal effects tend to average out the influence of the excess of defects. Experimental data from quasi-elastic neutron-scattering experiments[34,35] are also included in Table IV. However, it is important to note that only the values at 570 K are a direct experimental measurement. At higher temperatures diffusion constants have been calculated using an empirical Arrhenius equation fitted to measured values within a limited range of temperatures (523–723 K in Ref. 34 and 500–600 K in Ref. 35). Therefore comparisons with experimental values can only be semiquantitative, and it is somewhat difficult to assess the discrepancies between simulation and experiment.

VI. ELECTRONIC DENSITY OF STATES

In this section, we present a detailed study of the total electronic density of states (DOS), as well as the localization of the eigenstates measured in terms of the participation ratio, which is usually defined as

$$p_n = \frac{\left[\sum_i \sum_\alpha (C_{i\alpha}^n)^2 \right]^2}{\sum_i \left[\sum_\alpha (C_{i\alpha}^n)^2 \right]^2},$$
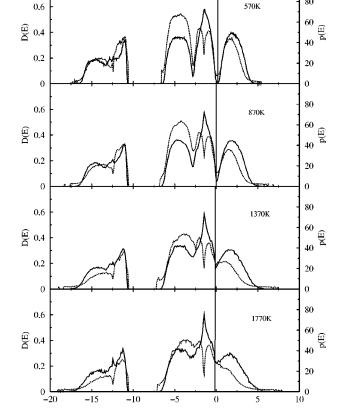$$(14)$$

where the numerator is simply the squared norm of the eigenvector corresponding to the eigenvalue ϵ_n. Thus the values of p_n defined in Eq. (14) are stored in discretized bins $[\epsilon_n, \epsilon_n + \delta\epsilon]$ for a given configuration, normalized according to the number of states present in the bin $[\epsilon_n, \epsilon_n + \delta\epsilon]$ and averaged over the simulation run. The DOS of solid trigonal and supercooled selenium are represented in Fig. 1. Calculated DOS for various states in the liquid phase are shown in Fig. 9. The state at 1770 K should correspond to an insulator, and in this case, our intention was to explore the ability of this simple TB model to reproduce the metal/nonmetal transition that occurs in Se when the temperature is further increased once the system has reached the metallic state. It has to be stressed that the DOS curves in disordered states have to be analyzed together with the participation ratio $p(E)$, since the latter provides a qualitative notion of the localization of eigenstates at given energies, and localization might alter the conducting character of the band structure. First, when we focus on the DOS of the trigonal phase, the main features we can observe concern the symmetry of the bands, as well as marked gaps, sharp edges, and narrow peaks (van Hove singularities), typical patterns of crystalline structures. The symmetry of the s band is associated to the presence of infinite chains and it is a well-known result of the moments theorem. In the same figure the local density of states calcu-

FIG. 9. TB-MD electronic density of states at various temperatures. Solid lines correspond to the DOS and participation ratios are denoted by dotted lines with their ordinates on the right.

lated in the LDA (Ref. 8) can be observed. Notice the good agreement obtained, which, as mentioned before, has proven to be a crucial condition to achieve a good fitting. Though the width of the p band is slightly overestimated, its shape is correct, which is much more important when temperature rises and the system melts. When this happens, van Hove singularities are smoothed out by topological disorder and band gaps shrink. Also, one observes an asymmetric deformation of the s band, as a consequence of chain distortion, together with a slight shift of the upper limit of the p band to higher energies. Another important effect is the narrowing of the central peak in the p band, associated to the nonbonding π orbitals, i.e., lone electron pairs. Nonetheless, the overall aspect of the DOS is preserved, which indicates that short-range interactions, mostly due to highly localized σ-covalent bonds between intrachain atoms, are largely preserved in the liquid. Our model reproduces reasonably well the semiconducting behavior and it predicts a smooth transition to a dirty metallic state, like the one at 1370 K. We have considered the system to be metallic when the participation ratio $p(E)$ is larger than 15 at the Fermi energy ϵ_f.

Note that $p(E)$ essentially follows the DOS since it is constrained by the fact that the states near the band edges are usually localized, i.e., $p(E) \to 0$ near edges and pseudogaps. Aside from this, one can see in Fig. 9 that the states near the

s and p orbital energies tend to be more localized, probably due to their nonbonding nature, a tendency that increases with temperature.

Finally, at 1770 K, we see that the system remains metallic, though the increase in temperature induces certain localization. In order to reproduce the metal/nonmetal transition the dimerization has to be correctly accounted for, which is not the case in our model. A proper representation of selenium under these physical conditions should include electron-electron correlations, both Coulombic and exchange-correlation terms, together with spin-spin interactions, which are expected to have a crucial role in stabilizing the dimers in the fluid at low densities.

VII. CONCLUSIONS

In this paper we have presented a tight-binding parametrization for Se, along the lines suggested by Goodwin, Skinner, and Pettifor.[20] The hopping integrals follow essentially the original parametrization suggested by Robertson[13] and pair repulsive forces and remaining parameters are determined to guarantee an optimum fit to *ab initio* cohesive energy curves for chains, rings, and crystal phases and the *ab initio* DOS of the trigonal phase. A series of TB-MD simulations with the proposed model has shown its ability to reproduce experimental structure factors from supercooled states to the vicinity of the critical point. The agreement with *ab initio* calculations is rather good, aside from a certain tendency to yield higher concentrations of defects at all temperatures. Finally, the TB model reproduces a semiconductor to metal transition when approaching the critical point, apparently induced by the breaking of the connected structures into relatively shorter chains, and very likely to the short bond lifetimes in the high-temperature states. In view of these results, future works should try to correct the deviations found for local coordinations in the amorphous and low-temperature liquid states, and this might be achieved by including terms in the Hamiltonian that minimize charge transfer, like the Hubbard Hamiltonian. As to the dynamic properties, a more detailed study of the chain dynamics, viscosities, and the vibrational spectrum will clearly need more representative samples and will be the subject of a forthcoming work.

[1] M. Edeling and W. Freyland, Ber. Bunsenges. Phys. Chem. **85**, 1049 (1981).

[2] R. Bellissent and G. Tourand, J. Non-Cryst. Solids **35-36**, 1221 (1980).

[3] M. Inui, K. Tamura, Y. Oh'ishi, I. Nakaso, K. Funakoshi, and W. Utsumi, J. Non-Cryst. Solids (to be published).

[4] K. Tamura and S. Hosokawa, Ber. Bunsenges. Phys. Chem. **96**, 681 (1992).

[5] D. Hohl and R.O. Jones, Phys. Rev. B **43**, 3856 (1991).

[6] F. Kirchhoff, M.J. Gillan, and J.M. Holender, J. Non-Cryst. Solids **205-207**, 924 (1996).

[7] G. Kresse, J. Furthmüller, and J. Hafner, Phys. Rev. B **50**, 13 181 (1994).

[8] F. Kirchhoff, G. Kresse, and M.J. Gillan, Phys. Rev. B **57**, 10 482 (1998).

[9] G. Kresse, F. Kirchhoff, and M.J. Gillan, Phys. Rev. B **59**, 3501 (1999).

[10] F. Shimojo, K. Hoshino, M. Watabe, and Y. Zempo, J. Phys.: Condens. Matter **10**, 1199 (1998).

[11] C. Bichara, A. Pellegatti, and J.P. Gaspard, Phys. Rev. B **49**, 6581 (1994).

[12] T. Koslowski, J. Phys.: Condens. Matter **9**, 613 (1997).

[13] J. Robertson, Adv. Phys. **32**, 361 (1983).

[14] S. Balasubramanian, K.V. Damodaran, and K.J. Rao, Chem. Phys. **162**, 131 (1992).

[15] M. García-Hernández, F.J. Bermejo, B. Fak, J.L. Martínez, E. Enciso, N.G. Almarza, and A. Criado, Phys. Rev. B **48**, 149 (1993).

[16] R. Mcgreevy and L. Pusztai, Mol. Simul. **1**, 359 (1988).

[17] V. Petkov and G. Yunchov, J. Phys.: Condens. Matter **8**, 1869 (1996).

[18] For a recent review, see, e.g., R.O. Jones and O. Gunnarson, Rev. Mod. Phys. **61**, 689 (1989).

[19] J.P. Perdew and Y. Wang, Phys. Rev. B **33**, 8800 (1986).

[20] L. Goodwin, A.J. Skinner, and D.G. Pettifor, Europhys. Lett. **9**, 701 (1989).

[21] W.A. Harrison, *Electronic Structure and the Properties of Solids* (Dover, New York, 1980).

[22] C.H. Xu, C.Z. Wang, C.T. Chan, and K.M. Ho, J. Phys.: Condens. Matter **4**, 6047 (1992).

[23] S. Hosokawa and K. Tamura, J. Non-Cryst. Solids **117/118**, 489 (1990).

[24] G. Kresse and J. Furthmüller, Comput. Mater. Sci. **6**, 15 (1996).

[25] D.J. Chadi and M.L. Cohen, Phys. Rev. B **8**, 5747 (1973).

[26] C.Z. Wang, C.T. Chan, and K.M. Ho, Phys. Rev. Lett. **66**, 189 (1991).

[27] R. Virkkunen, K. Laasonen, and R.M. Nieminen, J. Phys.: Condens. Matter **3**, 7455 (1991).

[28] Routine DSYEVD from LAPACK computer library. See *LAPACK Users' Guide*, 2nd ed. (SIAM, Philadelphia, 1995). This is not to be confused with the order-*N* diagonalization strategy proposed by Yang in the context of DFT calculations (Ref. 29).

[29] W. Yang, Phys. Rev. Lett. **66**, 1438 (1991).

[30] P. Ordejón, Comput. Mater. Sci. **12**, 157 (1998).

[31] L. Verlet, Phys. Rev. **165**, 202 (1968).

[32] See Refs. 8 and 9 for an analysis of clustering and defects with the effects of thermal vibrations removed.

[33] J.P. Gaspard, A. Pellegatti, F. Marinelli, and C. Bichara, Philos. Mag. B **77**, 727 (1998).

[34] A. Axmann, W. Gissler, A. Kollmar, and T. Springer, Discuss. Faraday Soc. **50**, 74 (1970).

[35] W.A. Phillips, U. Buchenau, N. Nücker, A.-J. Dianoux, and W. Petry, Phys. Rev. Lett. **63**, 2381 (1989).